DOI: 10.13009/EUCASS2023-550
Aerospace Europe Conference 2023 – 10TH EUCASS – 9TH CEAS

ReFEx: Reusability Flight Experiment - Aerothermodynamics

Divek Surujhlal[⋆†], *Viola Wartemann*[+] *and Alexander Wagner*[⋆]
[⋆]*DLR German Aerospace Center*
Bunsenstrasse 10, 37073 Göttingen, Germany
divek.surujhlal@dlr.de
[+]*DLR German Aerospace Center*
Lilienthalplatz 7, 38108 Braunschweig, Germany
Viola.Wartemann@dlr.de
[†]Corresponding author

Abstract

The Reusablility Flight Experiment (ReFEx) is currently under development at the German Aerospace Center (DLR). A coupled experimental and numerical campaign was carried out to investigate the surface heating on the ReFEx payload geometry consisting of a forebody and canard during reentry. In this way, numerical tools for a post-flight analysis can be preemptively improved where required. Experiments were undertaken at the High Enthalpy Shock Tunnel Göttingen (HEG) on a 1:4 scale model with the use of temperature sensitive paint (TSP) on the payload geometry to obtain surface heat flux. The model configuration was varied in angle of attack and canard deflection. A Reynolds-averaged Navier Stokes (RANS) solver in the DLR-TAU code was used for the numerical simulations. This investigation focused on the shock-shock interaction of the nose bow shock with the leading edge shock of the canards. This resulted in significant surface heat flux along the canard. Larger surface heat fluxes were measured in the experiments for the resulting flow downstream of the interaction on the canard, than obtained from the laminar RANS calculations. This was attributed to transition of the boundary layer within the interaction regions and in the presence of significant adverse pressure gradients. Other flow features along the forebody in the vicinity of the canard were qualitatively well-matched by the numerical solutions. This work aims to demonstrate the extent to which the numerical and experimental tools assist useful insights into flow phenomena at reentry conditions for a complex flight geometry, and the aspects for which improvements are required.

1. Introduction

The Reusability Flight Experiment (ReFEx) is intended to demonstrate aerodynamic control in the return phase of the trajectory of a reusable launch vehicle (RLV). The RLV comprises the first stage of a 3-stage vehicle, with a two-stage booster configuration. Given that cost-intensive payloads are foreseen to be packaged into the first stage, safe return of this stage is of paramount importance. A schematic of the first stage of the ReFEx vehicle is shown in figure 1.

There are currently two main methods for controlled return of first stage payloads. With vertical-takeoff-vertical-landing (VTVL), the payload is controlled during its return with a propulsion system. The development of a VTVL demonstrator is currently allocated to the scope of the CALLISTO Project within the DLR, CNES and JAXA Consortium. The second method is based on vertical-takeoff-horizontal-landing (VTHL) and is the subject of the ReFEx project. In this way, DLR is able to build scientific and technical expertise in the development and flight testing of both types of RLVs.

During the return phase of the flight experiment the first stage will be subject to a hypersonic freestream and is required to decelerate in a controlled manner to landing. This requires control surfaces (canards, see figure 1) on the forebody of the first stage. It is required to understand the aerothermodynamic loads on the forebody and canards due during high-speed reentry.
This work presents a joint experimental and numerical study that was conducted for further insight into the aerothermal loads at various configurations relevant to the return phase of the ReFEx trajectory. Experiments were conducted on a

DOI: 10.13009/EUCASS2023-550

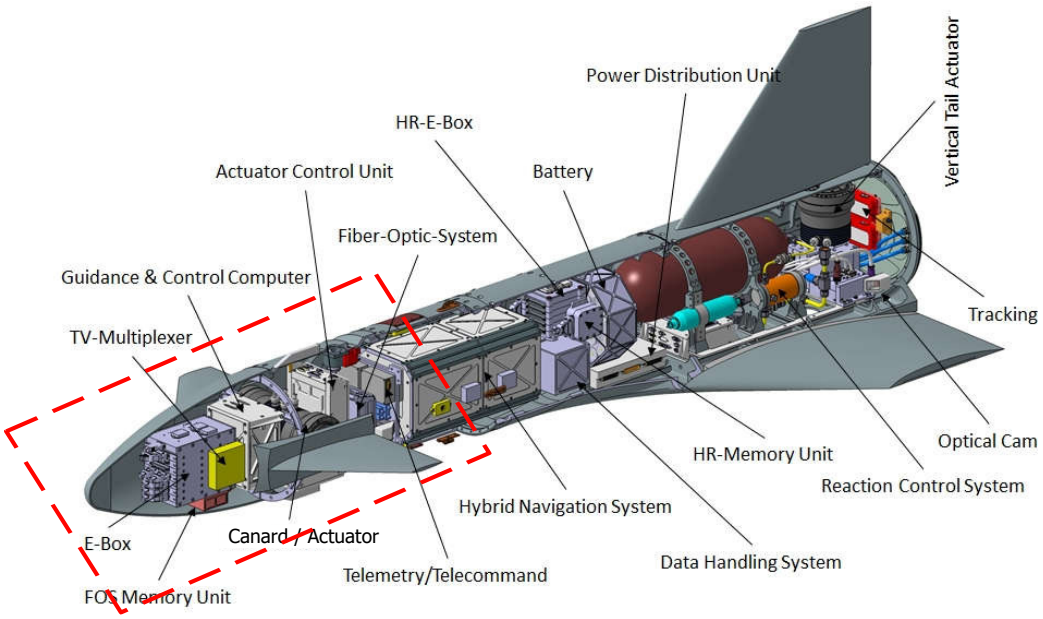

Figure 1: System overview of the ReFEx first stage as detailed by Bauer et al.[1] The payload section is indicated within the red box in the figure.

1:4 scale model with the intention to assist numerical re-building and specifically the prediction of flight vehicle heat loads. Such numerical models are foreseen for post-flight analyses.

2. Experimental details

2.1 HEG

The High Enthalpy Shock Tunnel Göttingen (HEG) was allocated for experimental testing of the ReFEx payload section. The HEG is a free-piston-driven shock tunnel and was commissioned for the simulation of hypersonic freestream conditions relevant to reentry conditions. More information on the HEG has been published by the DLR.[2]

In this work, results will be presented based on freestream conditions representative of atmospheric reentry up to 30 km altitude at Mach 7.4 with a stagnation enthalpy of approximately 3.0 MJ/kg. Table 1 presents relevant reservoir and freestream parameters for the condition used in this work.

Table 1: Selected nominal operating conditions of HEG at M = 7.4.

Condition	A
p_0 $[MPa]$	28.4
T_0 $[K]$	2582
h_0 $[MJ/kg]$	3.0
M_∞ [-]	7.4
T_∞ $[K]$	248
ρ_∞ $[g/m^3]$	43.2
u_∞ $[m/s]$	2350
Re_m $[1/m]$	6.4×10^6

2.2 Test geometry

The experiments at the HEG were focused on the ReFEx payload forebody and its control surfaces (canards). This geometry is indicated within the dotted box in figure 1. The objective was to quantify the surface heating loads experienced by the forebody during various configurations of the payload during flight. This meant that angles of attack,

DOI: 10.13009/EUCASS2023-550

carnard deflections and roll configurations (belly-up and belly-down) had to be considered. A subset of the results available to date are presented in this work.

The test model used for HEG experiments was a 1:4 scale model. Temperature sensitive paint (TSP) was the main diagnostic used from which surface heat flux on the forebody and a single canard was measured. A limited number of thermocouples (Type E, coaxial) and pressure transducers were placed on the model. These are indicated in figure 2.
Furthermore, the forebody was divided into two parts, one on which the instrumentation was installed (the green part

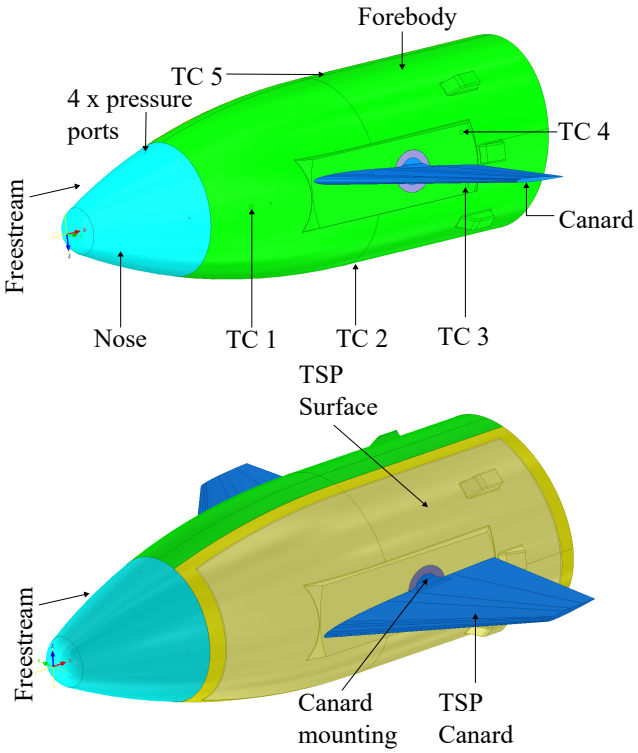

Figure 2: Overview of instrumentation and key features of the ReFEx forebody geometry. The left- and right- hand sides of the model are shown. Thermocouple positions are indicated by "TC".

in figure 2) and the surface onto which the TSP was applied, which included the canard. In order to replicate the flight geometry accurately, flight instrumentation ports and canard mounting structures were included in the test model and scaled accordingly from the flight geometry.

2.3 TSP and optical system

The base layer for the TSP was coated onto the model surface and machined to the model contour. The TSP was then applied to the base layer for each test. An important consideration of TSP coatings is that the base layer acts as an insulator to the model surface.[3] The base layer thickness was 100 μm and confirmed based on sample measurements along the model and canard. Figure 3 shows that, for the chosen base layer thickness, conduction of heat flux through to the model surface would happen after 7 ms and therefore after the tunnel test time. More details of TSP composition development can be found in the works of Schramm et al. and Ozawa et al.[3,4]

Given the complex three-dimensional ReFEx geometry, multiple cameras were set up around the HEG test section to capture the emission from the TSP surface at differnt angles. This meant that the model geometry can be three-dimensionally reconstructed and facilitate further comparison with results from three-dimemsional TAU computations.[5] The setup of the cameras in relation to the test section and model is shown in figure 4.

Surface heat-flux measurements were obtained from a temporal integration scheme of the temperature history for each pixel imaged from the measurement surface.[6] An in-situ calibration of the base layer following the procedures as detailed by Schramm et al.[3] and Ozawa et al.[4] was carried out. The base layer properties contained in the term $\rho_b c_b k_b$ was estimated for each camera system individually, given that the spectral response of the cameras were not all

DOI: 10.13009/EUCASS2023-550

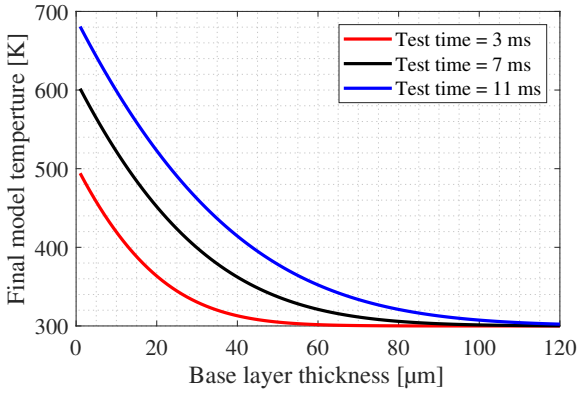

Figure 3: Thermal penetration depth chart showing possible base layer thickness as a function of model temperature at the end of tunnel test times of 3 ms, 7 ms and 11 ms for a constant heat flux of 2.0MW/m^2.

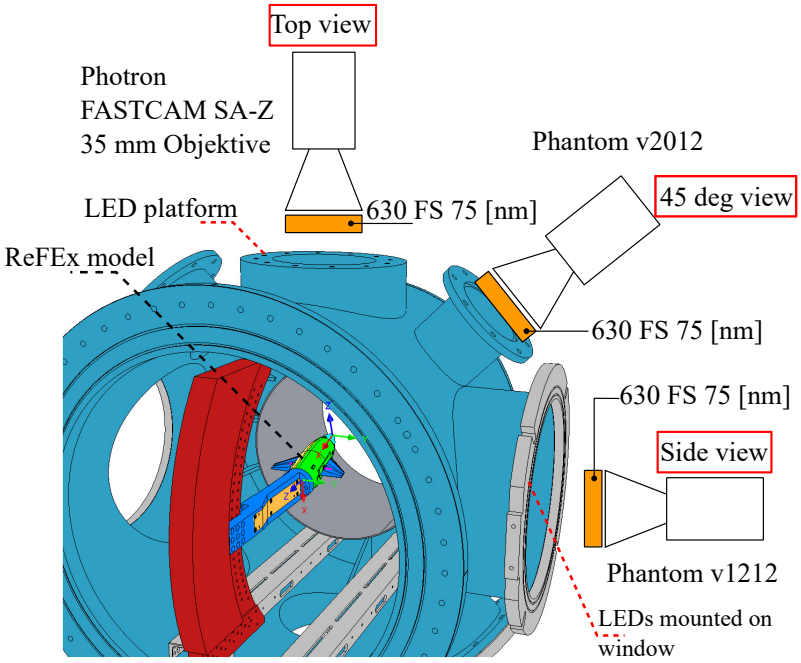

Figure 4: Overview of optical setup for image acquisition of TSP emission. Three high-speed cameras were mounted around the test section of HEG.

identical. Base layer property estimations are shown in table 2. The base layer property estimations were iteratively solved to within $\pm 32\ J/m^2Ks^{1/2}$ and the estimated uncertainty in the derived heat-flux was 5 %.[4]

2.4 Numerical modelling

The numerical results presented in the this paper are based all on Navier-Stokes simulations, using the flow solver TAU of the DLR. TAU is a three-dimensional parallel hybrid multigrid code and has been validated for hypersonic flows (see, e.g.: Reimann et al.,[7] Mack et al.[8] or Schwamborn et al.[9]). The investigated test cases were all conducted at a total enthalpy of approximately 3.0 MJ/kg (see table 1), at which the gas can be assumed to be perfect. The boundary layer state is defined as laminar. Due to the short measurement times of the HEG, the model wall temperature for all test cases is assumed to be isothermal at 293 K. Hybrid grids, using tetrahedrons and prisms, with about 11 million points are applied. The grids are especially clustered to the nose and the leading edges (see figure 5). The first layers of the boundary layer are arranged, that a linear temperature distribution from cell to cell is provided, beginning with the assumed cold wall.

DOI: 10.13009/EUCASS2023-550

Table 2: Base layer properties based on the term $\rho_b c_b k_b$ derived from in-situ calibration of the TSP with thermocouples located on the fuselage surface.

Camera (view)	Top	45 deg	Side
$\sqrt{\rho_b c_b k_b}$ $[J/m^2 K s^{1/2}]$	1035	2258	742

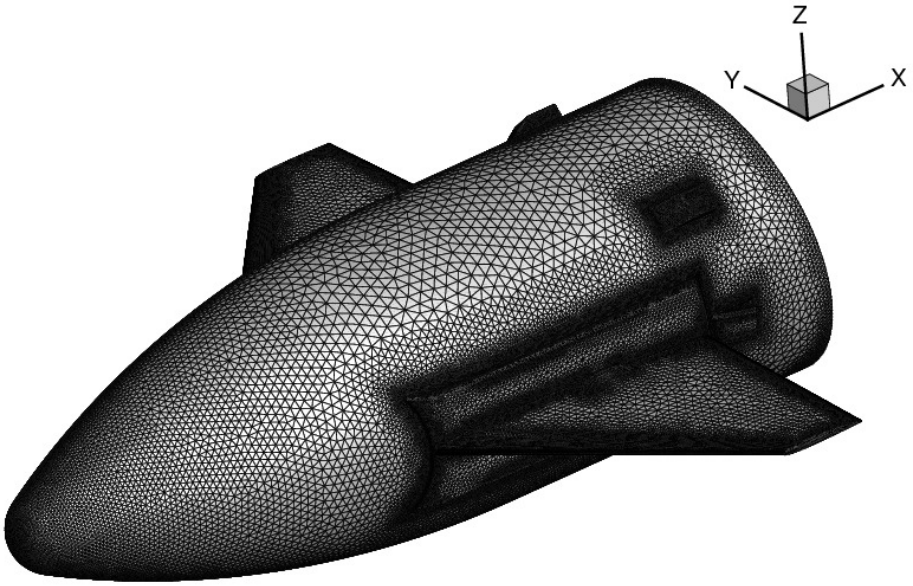

Figure 5: Example of surface grid

3. Results

3.1 Calibrated surface heat flux

As described in subsection 2.3, the proximity of the thermocouple TC 5 with the TSP surface on the forebody enabled an in-situ calibration of the base layer material properties, such that heat flux could be extracted from the TSP intensity images. The basis for this calibration was therefore the heat flux signal from the thermocouple. This is plotted in figure 6, also showing the mean and standard deviation bounds of the mean heat flux. In order to assess CFD validation of the surface heat flux, this was compared with the heat flux from the thermocouple, and is plotted in figure 6. The heat flux time signal from the thermocouple was filtered with a Savitzky-Golay filter with a window length of 101 samples and a polynomial of order 6. This shows that the CFD result somewhat underpredicted the mean heat flux measured by the thermocouple, but is within a single standard deviation of the mean. A comparison of the heat flux field derived from the TSP with that extracted from the CFD solution is shown for the case with the model body angle of attack (AoA) $\alpha = 0^\circ$ with canards at $\eta = 0^\circ$ in figure 7. Here, the canard angle (η) is defined relative to the body angle (α).

Along the forebody, there is a significant reduction in the heat flux in the downstream direction, corresponding to the favourable pressure gradient on the forebody and the expansion of the flow. This is reproduced in the numerical results. Both results in figure 6 show multiple shock/shock and shock wave/boundary layer interactions (SWBLIs) occurring in the vicinity of the canard. The result from the experiment displays a slight asymmetry due to the angle of the canard being adjusted to within $\pm 0.01^\circ$ An important difference is that the measured heat flux field in figure 7a shows significantly higher surface heat fluxes than the CFD result, in regions of reattachment of the flow on the forebody. These regions are marked A in figure 7a. This is due to transition of the boundary layer flow in the presence of large adverse pressure gradients. Related investigations on shockwave/boundary layer interactions (SWBLI) by Wagner et al. and Sandham et al.[10,11] confirmed that a transitioning boundary layer undergoing reattachment can result in a higher surface heat flux than during laminar reattachment. Boundary layer transition was not considered in the current CFD simulations.

It is also noteworthy that the reattachment of the flow outboard of the step on which the canard is mounted (marked B and C in figure 7a) is also a source of significant surface heat flux, which is again measured larger for the experiment

DOI: 10.13009/EUCASS2023-550

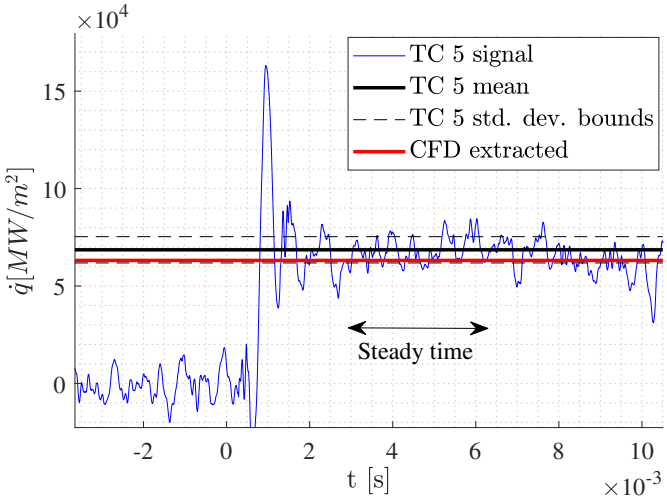

Figure 6: Time signal of the thermocouple TC 5, filtered with a Savitzky-Golay filter with a window length of 101 samples and polynomial order 6. This used for heat flux calibration of the TSP diagnostic. Mean and signal standard deviation bounds for the heat flux are also shown, as well as the value extracted from the CFD solution. Model AoA was $\alpha = 0° \pm 0.01°$ with canards at $\eta = 0° \pm 0.01°$.

than computed in the CFD result. A significant separation region is observed to exist upstream of the step mounting the canard and originating at the canard leading edge (marked S in figure 7a). This is well-described by the CFD result, matching the form of the separation region measured in the experiment. Overall, the CFD solutions were found to compare well qualitatively to the experimental results.

3.2 Overview of the shock-shock interaction at the canard

In order to obtain a broader impression of the flow around the ReFEx forebody, the 3-D field CFD solutions were examined, together with the different view perspectives obtained from different cameras mounted on the HEG test section (see figure 4).

A few main flow features were discussed pertaining to figure 7. In this section, particular examination is made of the shock-shock interaction at the canard. This interaction exists due to the interaction of the nose bow shock interacting with the leading edge shock of the canard. An overview of this situation is shown in figure 8.

The pressure contours plotted on the $z-$ plane show large pressure increases on the canard and it presents a critical location for examination of surface heat flux. The boundary layer development on the swept carnard is impacted by large adverse pressure gradients, and the possibility of separation makes this a critical vehicle surface from an aerodynamic perspective.

The canard shock-shock interaction was examined in the context of figure 9. In 8a, a pressure isosurface (with $p = 20\ kPa$) illustrates the bow shock generated at the nose of the forebody. This envelops the forebody, with supersonic flow downstream of the weak oblique portions of the shock. The supersonic flow downstream of the nose bow shock gives rise to a second shock generated at the leading edge of the both canards. The two shocks (nose bow shock and canard leading edge shock) interact leading to intense heating on the canard surface. This is examined in figure 9b which is extracted from the RANS CFD solution. The mean heat flux measured from the TSP is shown in figure 8c. This is a top view of the forebody and canard.

The canard leading edge heating is evident due to the presence of the leading edge shock. The TSP molecules reached their excitation limit and this meant that there was no signal obtained at the regions of excessive surface heat loads. The key features of the shock-shock interaction on the canard are labelled A, B and C. Feature A corresponds to the impingement of the nose bow shock with the canard leading edge shock. This results in intense heating in this region on the canard downstream of its leading edge. Due to the presence of this interaction, separation of the boundary layer is expected inboard of the shock impingement location at A. The resulting outboard reattachment of the boundary layer is labelled as feature B. This was confirmed by plotting the skin friction lines on the canard, as shown in figure

DOI: 10.13009/EUCASS2023-550

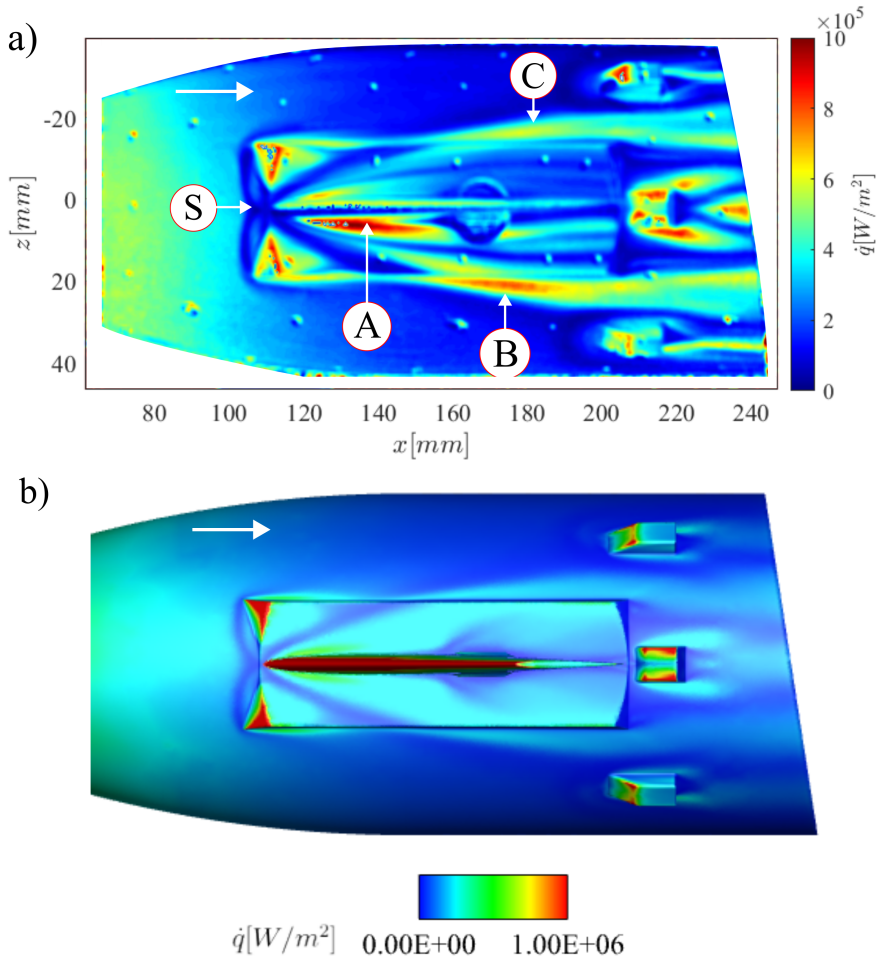

Figure 7: Field comparison of mean heat flux as calculated from TSP (above) and from the CFD solution for a model AoA $\alpha = 0°$ with canards at $\eta = 0°$. Colour mappings are based on the same scales. Freestream flow is from left to right, as indicated by the arrows at the top left of each subfigure.

10. The divergence of the streamlines corresponds to the reattachment zone[12] and resulted in an increased surface heat flux. This was shown to persist for a longer distance in the streamwise direction for the TSP data obtained from the experiment at HEG than shown in the CFD result. This is attributed to the possible transition of the boundary layer on the canard resulting in higher momentum of the reattached flow and non-localised heating shown in the experiment. The reattaching flow on the canard interacts with the outboard flow downstream of the leading edge shock and the difference in momentum of these two regions results in the development of a vortex, labelled as C in figure 9b and c. Lower surface heating was predicted by the CFD solution for the region C, but this is expected given that a fully turbulent flow on the canard was not considered in the current solutions.

3.3 Shock-shock interaction with variation in model configuration

Examination of the shock-shock interaction at the canard was carried out for model configurations with:

- Model AoA $\alpha = 0°$, canard angle $\eta = 15°$
- Model AoA $\alpha = 17.17°$, canard angle $\eta = 0°$

Here, the canard angle (η) is defined relative to the body angle (α).

Mean surface heat flux contours derived from the TSP data are shown in figure 11. The nose bow shock impingement on the canard is labelled A in figures 11a and b. In both cases, the leeside of the canard surface is viewed,

DOI: 10.13009/EUCASS2023-550

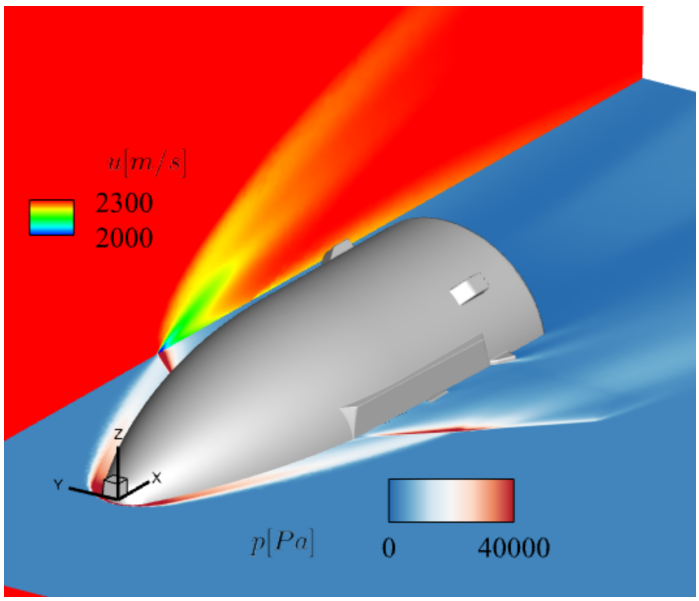

Figure 8: Overview of the shock-shock interaction involving the nose bow shock with the leading edge shock at the canard. The $z-$plane shows contours of pressure. The $y-$plane shows contours of streamwise velocity. Model AoA $\alpha = 0° \pm 0.01°$, canard angle $\eta = 0° \pm 0.01°$.

meaning that the flow is expanding over the canard upper surface. This results in a limitation of the regions of high heating due to the shock-shock interaction at the canard, as compared with figure 9c, for example. The reattachment vortex is marked B and appears differently based on model angle of attack. In figure 11a, the vortex B undergoes a gradual reduction in heat flux in the streamwise direction However, in figure 11b, the vortex B creates a large and persistent surface heating due to the stronger bow shock generated by the model with a considerably larger angle of attack ($\alpha = 17.17°$).

These points were qualitatively matched in the RANS CFD solutions shown in figure 12. For the case with a model angle $\alpha = 0°$ and canard angle $\eta = 15°$ (figure 12a), the surface heat flux created by the vortex B reduces slightly in the streamwise direction but is lower than that measured in HEG. This streamwise surface heat flux remains approximately constant for the case with a model angle $\alpha = 17.17°$ and canard angle $\eta = 0°$ (figure 12c), qualitatively consistent with the experimental observations from figure 11b. The underside of the canards (i.e the windward sides) display considerably larger surface heat fluxes, as shown in figures 12b and d, wherein the colour scales have been broadened in their range for clarity. These higher surface heat fluxes are due to the additional compression of the flow on the along canard underside.

4. Conclusion and outlook

An assessment of surface heat flux on a 1:4 scale model of the ReFEx payload geometry has been carried out in the High Enthalpy Shock Tunnel Göttingen (HEG). Surface heat flux was assessed with the use of temperature sensitive paint (TSP) applied on the forebody and on a canard. Qualitative agreement was found to exist between RANS CFD simulations carried out at the same conditions as the experiments. Multiple flow features around the canard and its mounting structure were captured by the simulations. From the experiments, an extreme heat flux on the leading edge of the canard resulted in a localised loss of signal from the TSP in these regions. Regarding the RANS CFD, under the constraint of a laminar boundary layer at all locations on the geometry, the high surface heat loads measured in the experiments were not quantitatively reproduced by the CFD results. This was examined in detail regarding the shock-shock interaction at the canard, involving the nose bow shock and the canard leading edge shock. The transition to turbulence and the complex separation and reattachment phenomena presents a difficulty for RANS simulations to fully predict certain regions of local heating in the context of these complex phenomena. It is important to note these limitations for the ReFEx geometry, for possible uncertainty reduction in post-flight numerical analyses. Qualitative comparisons were favourable and conclusions on spatial locations of regions of high surface heating agree with the experimental measurements.

DOI: 10.13009/EUCASS2023-550

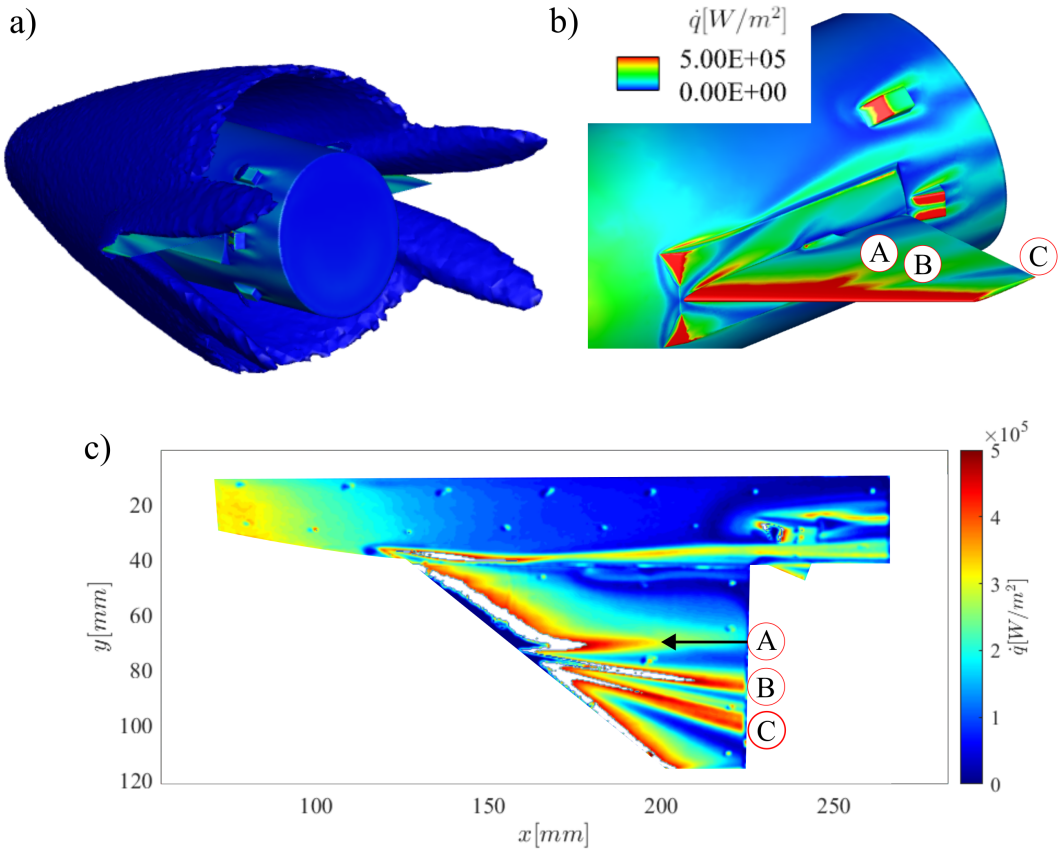

Figure 9: Detailed view of the shock-shock interaction at the canard. a) Isosurface of pressure ($p = 20kPa$) illustrating the nose bow shock and its envelopment of the ReFEx forebody as well as the diffraction of the shock surface due to the shock-shock interaction with the canard; b) Surface contours of heat flux on the forebody; c) Heat flux contours derived from TSP data showing the ReFEx forebody as viewed from the top. Freestream flow is from left to right. Model AoA $\alpha = 0° \pm 0.01°$, canard angle $\eta = 0° \pm 0.01°$.

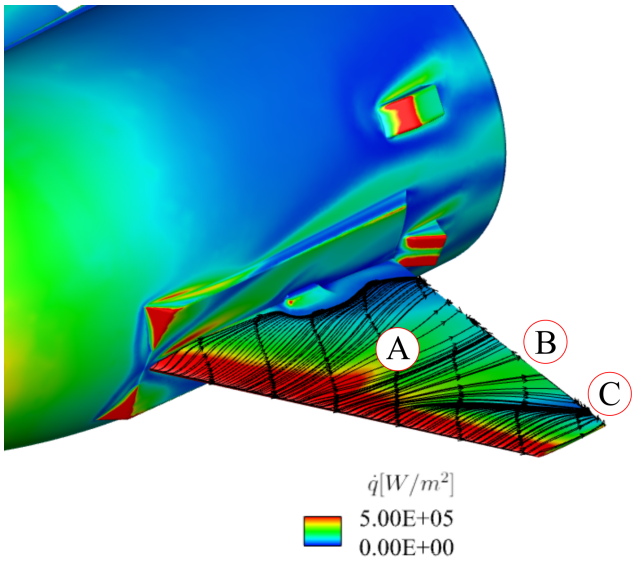

Figure 10: Detailed view of the shock-shock interaction at the canard with lines of skin-friction at the surface of the canard superimposed on contours of surface heat flux. Model AoA $\alpha = 0° \pm 0.01°$, canard angle $\eta = 0° \pm 0.01°$.

DOI: 10.13009/EUCASS2023-550

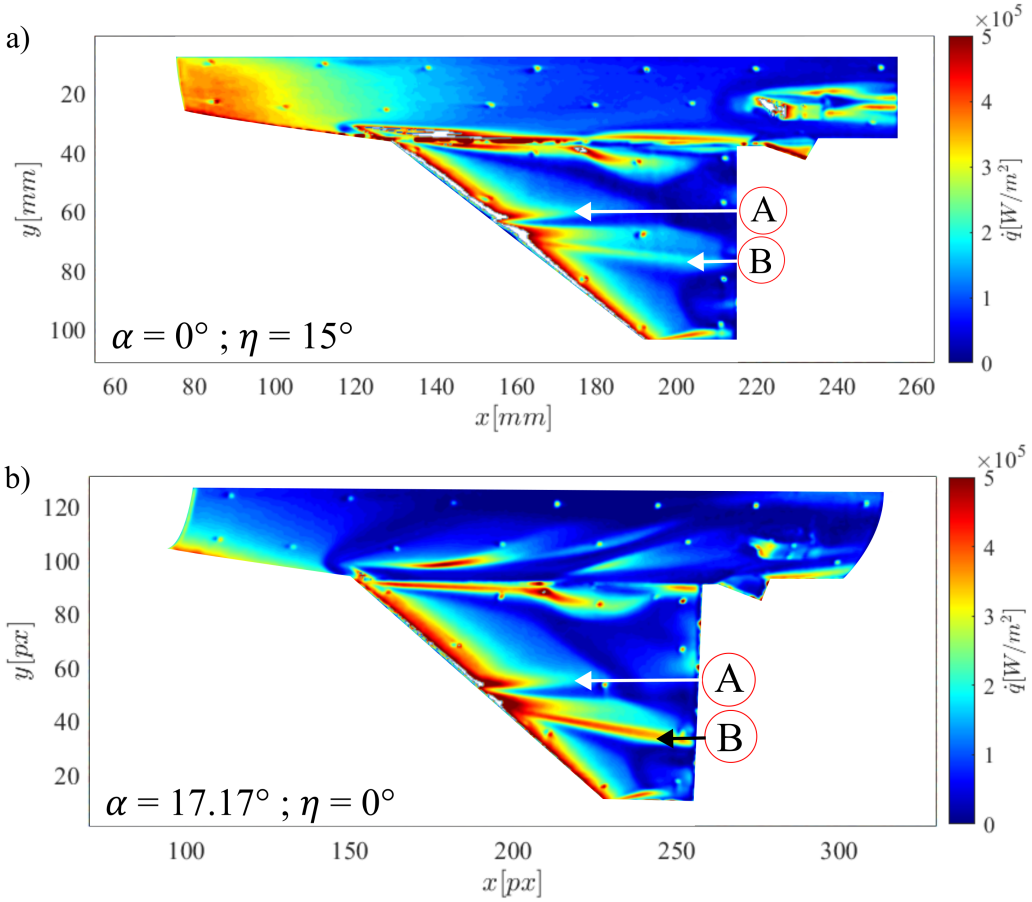

Figure 11: Overview of the surface heat flux on the canard derived from TSP with different configurations of the forebody. a) Model AoA $\alpha = 0° \pm 0.01°$, canard angle $\eta = 15° \pm 0.01°$; b) Model AoA $\alpha = 17.17° \pm 0.01°$, canard angle $\eta = 0° \pm 0.01°$. The canard angle (η) is defined relative to the body angle (α). Freestream flow is from left to right.

5. Acknowledgments

The authors wish to thank the technical staff at HEG, in particular Fabian Glasewald, Julian Ammer, Ingo Schwendtke and Uwe Frenzel, for their extensive preparations of the HEG and instrumentation of the test model.

DOI: 10.13009/EUCASS2023-550

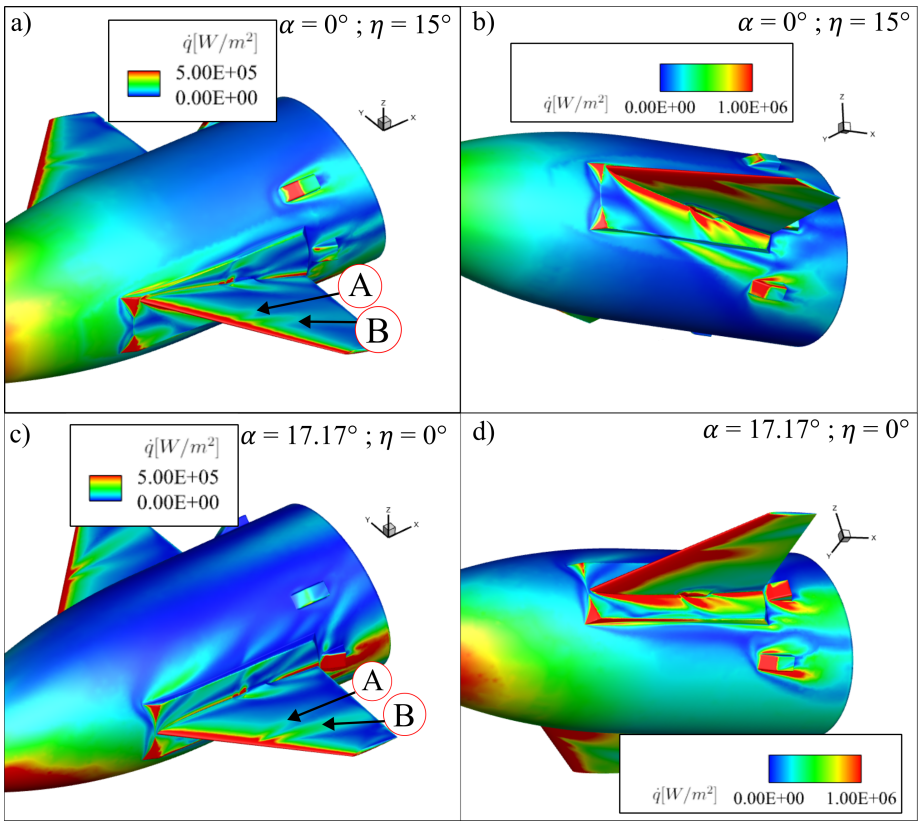

Figure 12: Overview of the surface heat flux on the canard with different configurations of the forebody. a), c) Model AoA $\alpha = 0° \pm 0.01°$, canard angle $\eta = 15° \pm 0.01°$; b), d) Underside of model with AoA $\alpha = 17.17° \pm 0.01°$, canard angle $\eta = 0° \pm 0.01°$. The canard angle (η) is defined relative to the body angle (α). Due to large heating of the canard underside, the colour scales of b) and d) were broadened accordingly.

References

[1] W. Bauer et al. DLR Reusability Flight Experiment ReFEx. *Acta Astronautica*, 168:57–68, 2020.

[2] Deutsches Zentrum für Luft - und Raumfahrt (DLR). The High Enthalpy Shock Tunnel Göttingen of the German Aerospace Center (DLR). *Journal of large-scale research facilities*, 4, A133, 2018.

[3] J. Martinez Schramm, K. Hannemann, H. Ozawa, W. Beck, and C. Klein. Development of temperature sensitive paints in the high enthalpy shock tunnel göttingen, HEG. In *8th European Symposium on Aerothermodynamics for Space Vehicles*, 2015.

[4] H. Ozawa, S. J. Laurence, J. Martinez Schramm, A. Wagner, and K. Hannemann. Fast response temperature sensitive paint measurements on a hypersonic transition cone. *Experiments in Fluids*, 56:1853, 2014.

[5] T. Ecker, J.M Schramm, L. Schmidt, D. Surujhlal, and A. Wagner. Shockwave boundary layer interaction of laminar/transitional flowpast a sharp fin. In *HiSST: 2nd International Conference onHigh-Speed Vehicle Science & Technology*, 2020.

[6] W. J. Cook, J. C. and E. J. Felderman. Reduction of data from thin-film heat-transfer gages - a concise numerical technique. *AIAA Journal*, 4(3):561–562, 1966.

[7] B. Reimann and V. Hannemann. Numerical Investigation of Double-Cone and Cylinder Experiments in High Enthalpy Flows Using the DLR TAU Code. In *48th AIAA Aerospace Sciences Meeting Including the New Horizons Forum and Aerospace Exposition*, 2010.

[8] A. Mack and V. Hannemann. Validation of the unstructured DLR-TAU-Code for hypersonic flows. In *32nd AIAA Fluid Dynamics Conference and Exhibit*, St. Louis, Missouri, 2002. AIAA 2002-3111.

DOI: 10.13009/EUCASS2023-550

[9] D. Schwamborn, T. Gerhold, and R. Heinrich. The DLR Tau-code: Recent applications in research and industry. In *European Conference on Computational Fluid Dynamics ECCOMAS CFD*, 2006.

[10] Alexander Wagner, Jan Martinez Schramm, Klaus Hannemann, Ryan Whitside, and Jean-Pierre Hickey. Hypersonic shock wave boundary layer interaction studies on a flat plate at elevated surface temperature. In *Shock Wave Interactions*, pages 231–243. Springer International Publishing, 2018.

[11] N. D. Sandham, E. Schülein, A. Wagner, S. Willems, and J. Steelant. Transitional shock-wave/boundary-layer interactions in hypersonic flow. *Journal of Fluid Mechanics*, 752:349–382, Jul 2014.

[12] Erich Schülein. Skin friction and heat flux measurements in shock/boundary layer interaction flows. *AIAA Journal*, 44(8):1732–1741, aug 2006.